Modelling and Experimental Validation of Grease Flow

Presented at the 28th ELGI Annual General Meeting 2016 Venice Italy

Author: Lars-Göran Westerberg[1*]
Co-Authors: Erik Höglund[2] and Chiranjit Sarkar[1†]
[1]Division of Fluid and Experimental Mechanics, [2]Division of Machine Elements
Department of Applied Sciences and Mathematics
Luleå University of Technology - Sweden
Lars-Goran.Westerberg@ltu.se

Lars is Associate Professor in Fluid Mechanics at Luleå University of Technology (LTU), Sweden. He has a M.Sc. in Space Engineering and a PhD in Fluid Mechanics from LTU. Lars has research- and educational experience from many engineering- and science areas from electromagnetism and space physics, to fluid mechanics, rheology and lubrication. Current research has a strong focus on lubricating greases and the relation between grease composition, rheology, and flow dynamics. Lars has over 60 scientific publications and have received the Edmond E. Bisson Award (2012) and Frank P. Bussick Award (2013) by the Society of Tribologists and Lubrication Engineers (STLE).
In addition to research and education, Lars has a couple of central leadership assignments at the university as Faculty Programme Director for the Master Programme in Space Engineering, and vice chairman for the Board of Employment.

Key words:
Grease flow; micro particle image velocimetry; boundary layer; velocity profile, lubrication; rheology, computational fluid dynamics (CFD); particle motion.

Abstract

Being able to fully model the flow dynamics of grease, including phase separation, will be highly valuable in the design of lubricated machine elements such as rolling element bearings. Complete models will also be a valuable tool in the process of providing tailor-made greases for different applications. An understanding of the grease flow dynamics enables prediction of grease distribution for optimum lubrication and for the migration of wear- and contaminant particles. In this paper the potential of combined analytical modelling, flow visualizations, and numerical modelling in grease flow dynamics is presented. Specifically, the relation between the rheology of the grease and its impact on the flow motion is of interest in combination with validation of the numerical models in simplified geometries. The numerical models then enable simulations in more complex geometries of particular interest for the grease and bearing industry. It is shown that grease flow is heavily influenced by its non-Newtonian properties and the shear rates in the contact, resulting in distinct regions of yielded and un-yielded grease. Further, the numerical models are shown to match well with experiments and analytical models, enabling numerical models on more complicated geometries.

1. Introduction

In many mechanical systems, the efficiency, expected life, reliability and maintenance costs are determined

by the quality of the lubrication of contacting surfaces. For lubrication, in general, lubricating oil or grease is used. There are clear advantages of using lubricating grease rather than oil; due to its *consistency*, grease does not easily leak out of the application and grease has inherent sealing properties. The latter reduces the demands on the design, a sealing system or improves its effectiveness thereby preventing the lubricant to leak into the environment. Other reasons to use grease are that it adheres to the surfaces, has good anti-corrosion properties and usually shows lower friction levels. Lubricating greases are used in many applications such as rolling bearings, gears, rail-wheel lubrication, hub-units for trucks, and passenger cars. In fact, grease is used as lubricant in 80-90% of all rolling bearings (Lugt, 2016).

The main drawback of grease lubrication is that the life- of grease is shorter than the expected life of the machine element, requiring re-lubrication. Optimum lubrication of surfaces in contact means that a lubricant film is formed fully separating the surfaces. If the surfaces are moving, such as in the contact between ball and races in a bearing, the lubricant is sheared in the gap between the surfaces. The load in the contact creates a pressure on the film leading to lubricant leakage transverse to the running direction, gradually reducing the available amount of lubricant. Therefore, the running track needs to be replenished continuously in order to maintain a sufficiently thick lubricating film. In the case of oil lubrication this is usually not a problem. Oil is a viscous material which easily flows and replenishes the surfaces of the loaded contacts in gears and bearings.

Grease is thickened oil, i.e. a multiphase system consisting of a thickener, base oil and additives (Gow, 1994). Typical greases contain 70-90% oil, 3-30% thickener, and additives – even though the distinction between the base oil and additives is not always clear as mixtures of fluids often are used (Lugt, 2013). Lubricating grease is a visco-elastic material showing yield behaviour (Gow, 1991), meaning that in the absence of a threshold force the grease will not flow. This is also the main problem compared to oil lubrication: once the grease is pushed to the side of the contacts it does not readily flow back into the track.

For grease lubricated systems, the initial filling is of crucial importance. After the filling, the grease is forced to flow by the moving elements such as gear teeth or rolling elements (this flow is generally referred to as *churning*). Most of the grease is pushed sideways; part of it stays close to the contacts or, in the case of rolling bearings ends up on the cage. The grease directly participates in the lubrication of the above mentioned loaded contacts but will also bleed oil and replenish the tracks (Baart et al., 2009)). Too much grease will lead to excessive churning and therefore, because of the relatively high consistency of grease, cause high friction levels, leading to high operating temperatures (Vikström and Höglund, 1996). Mechanical and thermal loads will cause breakdown of the thickener structure and oxidation of the oil leading to a reduced grease life. Too little grease on the other hand reduces the replenishment of the running tracks and therefore shortens life of the lubricated component.

Lugt et al. (2009) showed that in addition to the amount of grease, also the initial position of the grease in the bearing or gearbox before churning is important. Relatively small differences in initial filling may lead to large differences in performance. The ultimate aim is to provide the system with a grease *distribution* that is optimal for the system performance. To prevent the grease from continuously flowing, too much grease cannot be applied. To ensure optimal lubrication, too little grease cannot be applied. The grease distribution is formed during the first hours of operation when the initial grease filling is *flowing* inside the bearing.

The flow of grease is determined by its rheological properties in combination with, e.g., vibrations, temperature and with the material and roughness of the elements carrying the grease, such as seals, cages, rolling elements and rings. In particular, grease flow behaviour close to the surfaces of these elements has shown to be of interest and especially the existence and origins of wall slip, i.e. slip between the solid surface of the component and the grease. Bramhall and Hutton (1960) and Vinogradov et al. (1970) have argued that wall slip occurs on a layer of oil due to the lower concentration of thickener at the wall. Bramhall and Hutton (1960) introduced a model assuming a low viscosity layer near the wall and calculated a layer thickness of about 0.05 µm for smooth lithium-based greases. Czarny (2002) concluded that there exists a concentration gradient of thickener close to the wall due to the interactions between the grease thickener and the wall which results in the formation of a thickener wall layer, with on top of this, an oil layer.

Rolling bearings are normally filled with about 30% grease to avoid heavy churning and in the bearing both wall-bounded- and free-surface flows are present. The latter has been addressed in the literature for the case of oil flow. Gershuni et al.

(2008) and van Zoelen et al. (2008) developed models and experimentally studied oil flow in bearings by means of centrifugal force induced flow of thin layers. Such models have also been developed for the very complex flow in full rolling bearings with multiple bodies and layers (van Zoelen (2010)); see Fig. 1. Larsson et al. (1994) modelled the formation of grease and oil droplets forming at the outlet of concentrated contacts.

Understanding and ultimately being able to model the grease flow dynamics presented above in varying geometries, enables prediction of grease distribution for optimum lubrication and for the migration of wear- and contaminant particles. Complete grease flow models including phase separation will be a highly valuable tool in the design of lubricated systems as well as enabling tailor made greases for different applications. In this paper the potential of combined analytical modelling, flow visualizations, and numerical modelling in grease flow dynamics is presented. Specifically, the relation between the rheology of the grease and its impact on the flow motion is of interest in combination with validation of the numerical models in simplified geometries. The numerical models then enable simulations in more complex geometries of particular interest for the grease and bearing industry.

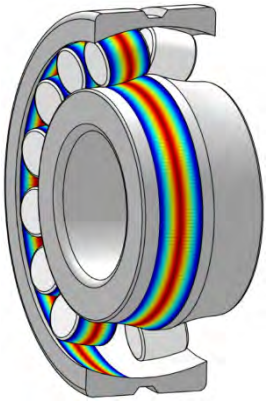

Figure 1: Oil layer distribution on a spherical roller bearing where the oil flow is induced by the tangential component of the centrifugal forces on inner ring and rollers (van Zoelen, 2010). Red colour indicates the thinnest lubricant film.

2. Methods

In this paper two different flow situations have been studied, a straight channel without and with restrictions respectively; see Fig. 2. Numerical modelling with Computational fluid Dynamics (CFD) is presented together with analytical modelling and flow visualizations using micro Particle Image Velocimetry (μPIV). Three lithium-soap (lithium hydroxy stearate) greases have been considered. Using a cone-plate rheometer, their rheology (apparent viscosity) has been modelled using the Herschel-Bulkley rheology model (Eq. 1; Tab. 1). The Herschel-Bulkley model reads

$$\eta(\dot{\gamma}) = \frac{\tau_0}{\dot{\gamma}} + K\dot{\gamma}^{n-1}, \qquad [1]$$

where η is the apparent viscosity, τ_0 the yield stress, K the consistency index, n the shear thinning/thickening (Power law) exponent – which for a shear thinning material like grease is less than one, and $\dot{\gamma}$ the shear rate.

Table 1: Data from a cone-plate rheometer for the three lithium-soap greases used based on the Herschel-Bulkley rheology model (Eq. 1). Values in brackets are fitted values for the analytical model; see §2.1 and §3.

	τ_0[Pa]	K[Pa·sn]	n[-]	Base oil viscosity(Pa·s)
NLGI 00	0	1.85 (4.9)	1	0.89
NLGI 1	189 (700)	4.1 (42)	0.797	0.49
NLGI 2	650 (1200)	20.6 (165)	0.605	0.25

2.1 Analytical modelling

In the modelling of grease flow the equation of motion is considered, which on vector form reads

$$\rho\frac{D\mathbf{u}}{Dt} = \rho\frac{\partial\mathbf{u}}{\partial t} + \rho(\mathbf{u}\cdot\nabla)\mathbf{u} = -\nabla p + \rho\mathbf{F} + \nabla\cdot\tau\,. \qquad [3]$$

Here D/Dt is the material derivative, p the pressure, ρ the grease density, τ the stress matrix/tensor, and **F** a volume force – which typically is gravity but in general can be any volume force such as centrifugal forces or electromagnetic forces. For a given model describing the relation between the shear rate and shear stress, the equation of motion goes under the name Navier-Stokes equation. To illustrate how to solve the equation of motion we consider the flow in a straight channel (Fig. 2a). The length scale of the channel is such that the variation in the flow direction (x) and in/out of the plane (z) is much smaller compared to the direction normal to the flow direction (y), i.e. going in the direction from the bottom boundary to the top boundary. This yields a one-dimensional flow velocity $\mathbf{u} = u_x(y)\mathbf{x}$; **x** being the unit vector pointing in the x-direction. The only non-zero components of the shear stress tensor are τ_{xy} and τ_{yx} which according to the symmetry property of the stress tensor are equal. Considering a stationary flow ($\partial/\partial t = 0$) Eq. [3] then yields (Westerberg et al. 2010)

$$\frac{dp}{dx} = \frac{d\tau}{dy}. \qquad [4]$$

The relation between the shear stress and shear rate ($\dot{\gamma}$) is for a generalized Newtonian fluid described by

$$\tau_{ij,j} = \eta(\dot{\gamma})\dot{\gamma}_{ij}, \qquad [6]$$

where η is the shear rate-dependent viscosity and $\dot{\gamma}_{ij} = \nabla u - \nabla u^{T}$ the shear rate tensor, relating to the scalar shear rate as

$$\dot{\gamma} = \sqrt{\frac{1}{2}\sum_{i}\sum_{j}\dot{\gamma}_{ij}\dot{\gamma}_{ij}}. \qquad [7]$$

For the present 1D flow Eq. [7] yields

$$\dot{\gamma} = \frac{du}{dy}, \qquad [8]$$

where $u = u_x(y)$. For a Herschel-Bulkley fluid (Eq. [1]) we then get

$$\frac{dp}{dx} = K\frac{d}{dy}\left(\frac{du}{dy}\right)^{n} = const. \qquad [9]$$

Rearranging and integrating once results in

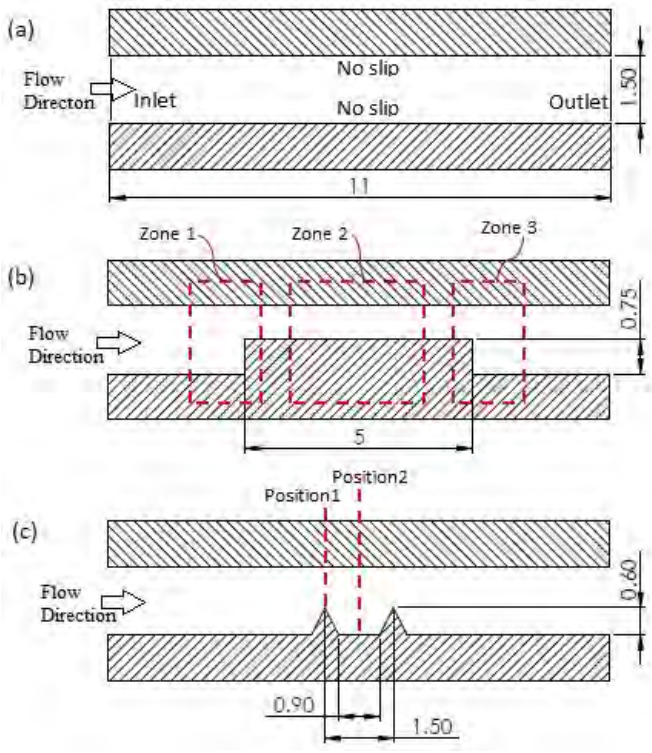

Figure 2: Progression of straight channels used in the CFD modelling for validation with flow visualizations: without restrictions (a - also used in the analytical modelling part), step restriction (b), and a double lip restriction (c). Measures in mm.

$$\left(\frac{du}{dy}\right)^{n} = \frac{1}{K}\frac{dp}{dx}y + C_1. \qquad [10]$$

To determine C_1 we consider the force balance at the walls implying that the friction force should be equal to the driving pressure force, according to

$$\left[\tau_0 + K\left(\frac{du}{dy}|_{y=0}\right)^{n}\right]2dL = \Delta p \cdot dh, \qquad [11]$$

where the term in square brackets is the wall shear stress, d is the width of the channel, h is the height of the channel, L is the length of the channel, and Δp is the pressure drop. Using

$$-\frac{\Delta p}{L} = \frac{dp}{dx} \qquad [12]$$

gives

$$\left(\frac{du}{dy}|_{y=0}\right)^{n} = -\frac{1}{K}\left(\frac{h}{2}\frac{dp}{dx} + \tau_0\right). \qquad [13]$$

Eq. [10] and Eq. [13] then gives

$$C_1 = -\frac{1}{K}\left(\frac{h}{2}\frac{dp}{dx} + \tau_0\right), \qquad [14]$$

resulting in

$$\left(\frac{du}{dy}\right)^{n} = \frac{1}{K}\frac{dp}{dx}y - \frac{1}{K}\left(\frac{h}{2}\frac{dp}{dx} + \tau_0\right). \qquad [15]$$

As presented above, the fluid behaves as a solid in the regions where the stress becomes lower than the characteristic yield stress, τ_0. Considering the velocity profile across the channel, this means that the velocity becomes constant at a certain y-value, here denoted y_l. In order to obtain y_l consider the location where the velocity is constant, i.e.

$$\left(\frac{du}{dy}\Big|_{y=y_l}\right)^n = \frac{1}{K}\frac{dp}{dx}y_l - \frac{1}{K}\left(\frac{h}{2}\frac{dp}{dx} + \tau_0\right) = 0 \,. \qquad [16]$$

Solving for y_l gives

$$y_l = \frac{h}{2} + \frac{\tau_0}{\frac{dp}{dx}} \,. \qquad [17]$$

For a Newtonian fluid, $\tau_0 = 0$, giving $y_l = h/2$, which corresponds to a parabolic velocity distribution. Figure 3 shows that the y_l-value increases with increasing pressure, and/or decreasing NLGI number of the grease. According to Eq. [17] the y_l value is given by the reciprocal pressure gradient. For an infinite pressure gradient $y_l = h/2$, giving a parabolic velocity profile. The velocity profile for the NLGI 00 grease remains unaffected by the increase of pressure drop (already having a Newtonian behaviour at low pressure drop due to a negligible yield stress value). The effect of the pressure drop on y_l is shown for the greases with NLGI grade 1 and 2 respectively, as the length of the plug region decreases with increasing pressure drop (equivalent to an increasing y_l value). This is in line with the rate of shear dependent behaviour of grease, where at low shear rates the viscosity of the grease equals the bulk grease viscosity, while for infinite shear rates the grease viscosity approaches the base oil viscosity which has a Newtonian rheology (Lugt, 2013).

To obtain the velocity as a function of position (y), Eq. [15] is integrated, resulting in

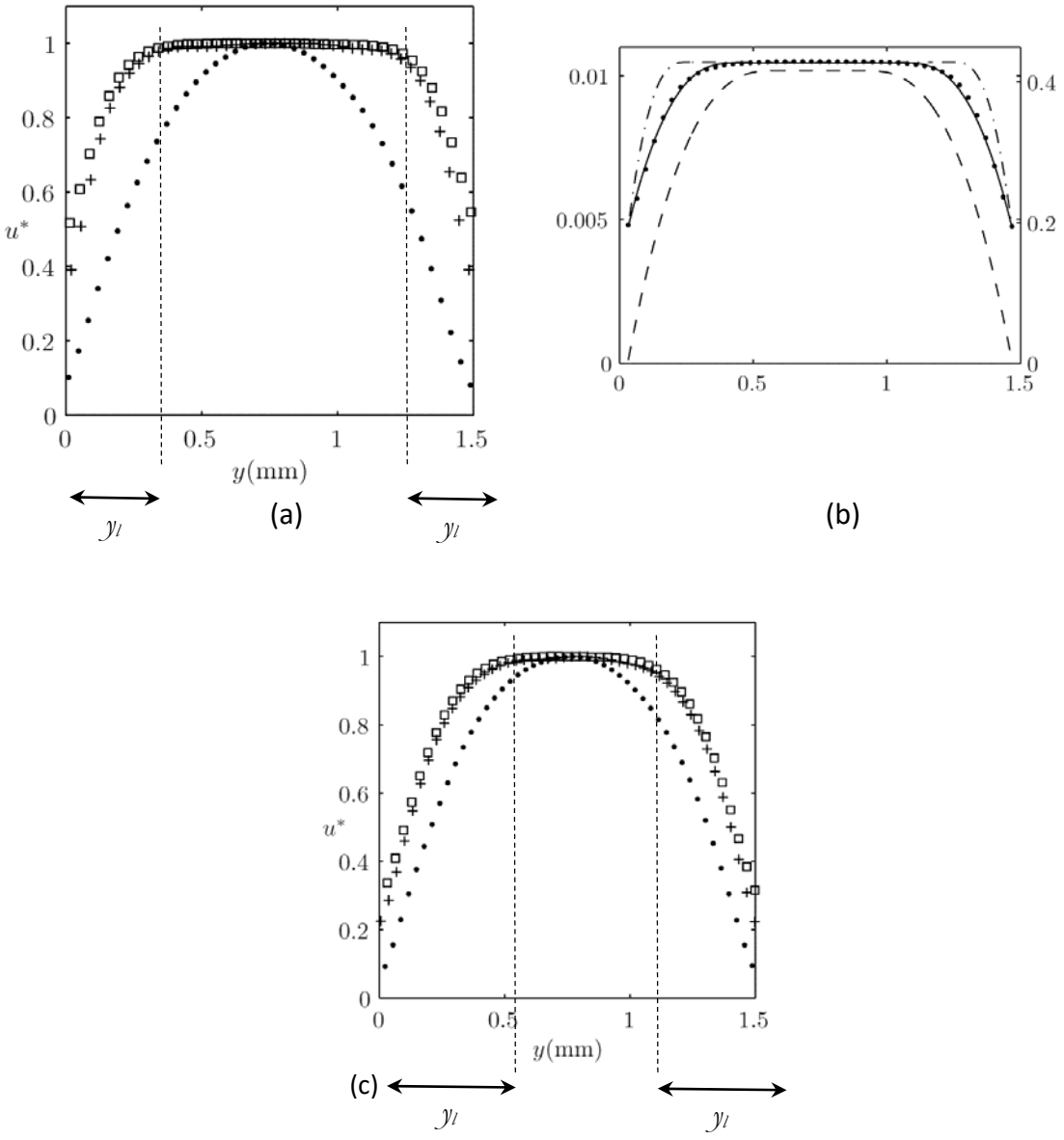

Figure 3: (a) Velocity profiles from flow visualizations across a straight channel without restrictions for three lithium greases with different thickness; see Tab. 1 for rheological data. The different labels represent different grease thickness such that □: NLGI 2, +: NLG I1, and •: NLGI 00. y_l denotes the distance to the yield point. (b) Velocity profiles across a straight channel of width 1.5 mm. The profiles show dimensionless quantities, scaled with the

maximum velocity value. All curves except the dash-labelled one have their scale on the left *y*-axis. *Dotted*: Velocity profile obtained from the μPIV measurements. *Solid*: analytical velocity profile with adapted τ_0 and K values, and measured driving pressure gradient. *Dash-dotted*: analytical velocity profile using the measured values of the rheological parameters and an *adapted* value of the pressure gradient. *Dashed*: analytical velocity profile using the measured values of the rheological parameters and the pressure gradient. (c) Same as in (a) but with higher driving pressure (pressure drop). From Westerberg et al. (2010).

$$u(y) = \frac{n}{n+1}\frac{1}{\frac{1}{K}\frac{dp}{dx}}\left[\frac{1}{K}\frac{dp}{dx}\left(y-\frac{h}{2}\right)-\frac{\tau_0}{K}\right]^{\frac{n+1}{n}} + C_2, \qquad [18]$$

where C_2 is determined from the slip condition at a distance y_s from the wall, i.e. $u(y = y_s) = u_s$ - where u_s is the slip velocity, giving

This results in the following expression for the velocity profile

$$C_2 = u_s - \frac{n}{n+1}\frac{1}{\frac{1}{K}\frac{dp}{dx}}\left[\frac{1}{K}\frac{dp}{dx}\left(y_s-\frac{h}{2}\right)-\frac{\tau_0}{K}\right]^{\frac{n+1}{n}}. \qquad [19]$$

$$u(y) = \frac{n}{n+1}\frac{1}{\frac{1}{K}\frac{dp}{dx}}\left[\frac{1}{K}\frac{dp}{dx}\left(y-\frac{h}{2}\right)-\frac{\tau_0}{K}\right]^{\frac{n+1}{n}} - \frac{n}{n+1}\frac{1}{\frac{1}{K}\frac{dp}{dx}}\left[\frac{1}{K}\frac{dp}{dx}\left(y_s-\frac{h}{2}\right)-\frac{\tau_0}{K}\right]^{\frac{n+1}{n}} + u_s, \qquad [20]$$

which is valid in the region $y_s \le y \le y_l$. The problem is symmetrical in $y = h/2$. Therefore the velocity in the corresponding upper region is

$$u(y) = \frac{n}{n+1}\frac{1}{\frac{1}{K}\frac{dp}{dx}}\left[\frac{1}{K}\frac{dp}{dx}\left((h-y)-\frac{h}{2}\right)-\frac{\tau_0}{K}\right]^{\frac{n+1}{n}} - \frac{n}{n+1}\frac{1}{\frac{1}{K}\frac{dp}{dx}}\left[\frac{1}{K}\frac{dp}{dx}\left(y_s-\frac{h}{2}\right)-\frac{\tau_0}{K}\right]^{\frac{n+1}{n}} + u_s, \qquad [21]$$

which in turn in valid in the region $h - y_l \le y \le h - y_s$. When $y_l < y < (h - y_l)$ the velocity is constant. The maximum velocity then reads

$$u_{\max.} = u(y = y_l) = u_s - \frac{n}{n+1}\frac{1}{\frac{1}{K}\frac{dp}{dx}}\left[\frac{1}{K}\frac{dp}{dx}\left(y_s-\frac{h}{2}\right)-\frac{\tau_0}{K}\right]^{\frac{n+1}{n}}. \qquad [22]$$

The velocity profile is shown in Fig. 3b. As shown it is possible to get a good fit between measured values and the analytical profile. Interestingly, in order to get a good fit the measured values of the rheological parameters have to be adjusted when applied to the model, implying possible errors in the rheology measurements. As discussed in Westerberg et al. (2010) this is possibly due to slip close to the walls which not is implemented in the models used in rheometer's to calculate the parameter values.

To conclude this part, it is possible to solve the governing equations by means of the velocity across the channel width. The location of the yield point in the flow is also obtained, and wall slip is possible to also include in the model.

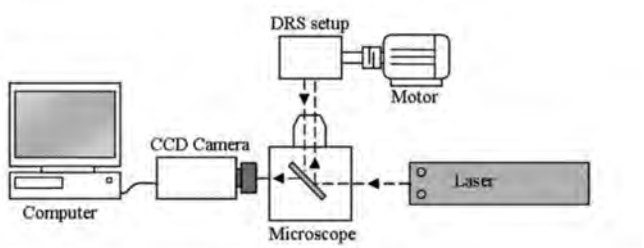

Figure 4: A typical µPIV setup with microscope, camera, test rig, motor/pump to drive the flow, laser, and computer.

2.2 Flow visualizations using micro Particle Image Velocimetry (µPIV)

2.2.1 Principles of PIV

PIV is a straightforward method to capture the flow motion of a medium: images of a particle seeded flow are taken by a high speed camera, Fig. 4. As light source a pulsed laser is used; and the laser is synchronized with the camera in order to capture images separated by a small time step; see Fig. 5. The tracer particles are illuminated in a single plane of the flow with a light sheet whose thickness is less than the depth of field of the image recording system (Meinhart et. al., 2000). For the measurements in this paper, particles with a diameter of 7.68 μm ± 0.19 μm and 3.23 μm±0.06 μm has been used. The particle motion, and ultimately the flow motion, is traced using a correlation algorithm; see e.g. Westerberg et al. (2010) for more details about µPIV.

2.2.2. Flow visualizations in straight channels

A progressive approach has been considered, going from the flow in a straight channel without restrictions to a straight channel with a step- and double lip restriction respectively (Fig. 2). This approach serves both the fundamental understanding of lubricating grease flow dynamics (including the motion of contamination- and wear particles in the grease flow), and also for experimental validation of numerical models. This is of specific importance in the ambition to model the full flow in varying grease lubricated geometries.

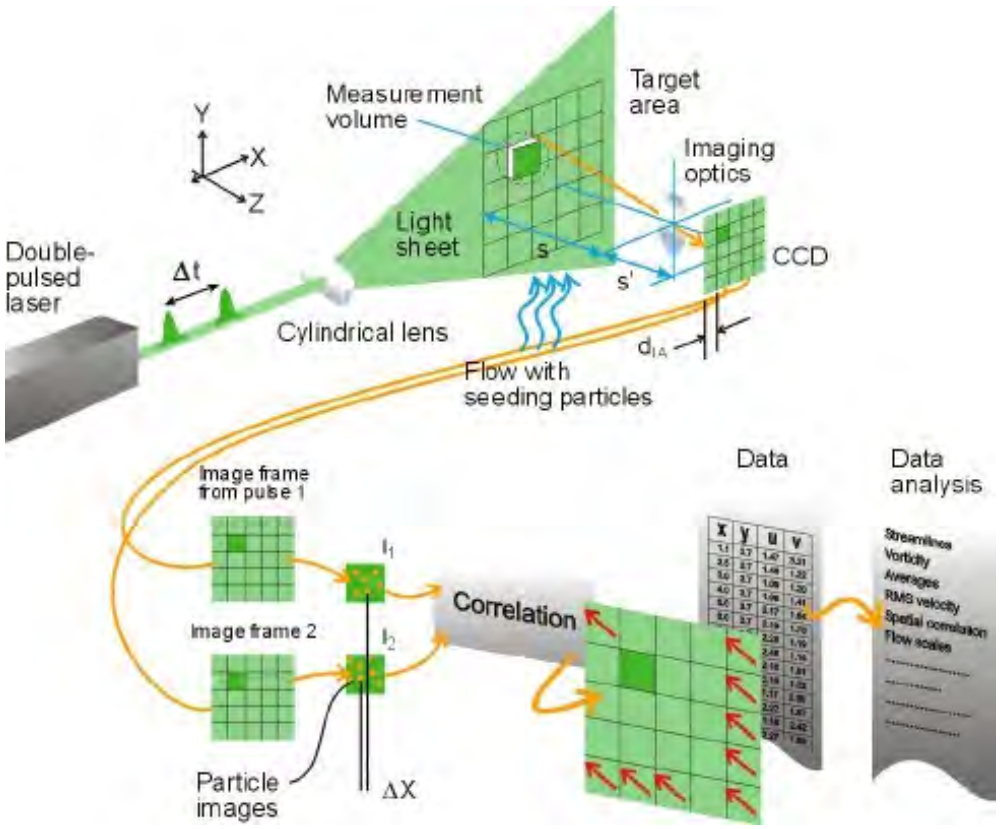

Figure 5: The principle of PIV. The correlation between images is made via Fast Fourier Transform (FFT) in the PIV software. The calculations does hence not track individual particles, but capture the statistical behaviour of all particles in the sub-frames (interrogation areas) of each image.

2.3 Numerical modelling of lubricating grease flow using Computational Fluid Dynamics (CFD)

CFD is a powerful tool for modelling flow and its potential has grown in hand with the general computational capacity. The concept behind CFD is to numerically solve the equations governing the flow by to the domain apply a computational grid (*mesh)*; i.e. the flow domain (channel in the present case) is divided in to a number of computational cells/elements, where at the nodes connecting the cells, the discrete governing equations are solved. A fundamental constraint of CFD – as with all numerical modelling – is that the result is an approximation; limitations to the model apply to the size, form, and distribution of the elements together with the formulation of the problem (boundary conditions and turbulence models for instance) and solver techniques. It is therefore of utmost importance to have experimental data, and if possible, analytical solutions to validate the accuracy of the numerical model.

The approach in this paper and in the ongoing work on flow motion of lubricating grease is to build numerical models for the cases which have been analysed in terms of flow visualizations. By comparing the numerical results with µPIV data and analytical models a rigid foundation of the quality and trust of the obtained results is built. This ensures that the model itself works, that the rheology model is representative, and that the solution is valid. With this foundation more complex geometries can be approached.

As mentioned in the introduction, grease is a complex semi-fluid due to its multi-phase composition, and modelling the full phase composition is a challenge. In fact, CFD analysis of lubricating grease flow is in general very scarce in the literature; corresponding models for lubricating oils are more frequently occurring, see e.g. Mashoor et al. (2013) for one study on the topic.

2.3.1. The grease yield behaviour and how to model it numerically

In this paper the grease is as a first order approximation treated as a single-phase continuous medium, described by the Herschel-Bulkley rheology model (Eq. 1). The H-B model is in all its simplicity practical to use as analytical solutions are possible to obtain (Eq. [22]) and it is also commonly used in the lubrication community. It is however an engineering model (Lugt, 2013). The yield behaviour is not discontinuous as indicated by Eq. 1; i.e. physically there is no singular value of the shear stress, τ_0 at which the grease instantly changes from being continuously sheared, to not being sheared at all and consequently move as a solid body (plug). The grease yield behaviour origins in the visco-elastic properties of the material: for sufficiently low shear rates the grease acts as an elastic, solid body, while as the shear rate increases the grease will reach its plasticity (yield) limit and start to continuously deform. The transition from elasticity to plasticity is in turn continuous, yielding a non-singular yield stress value. It works well though as an engineering model. Treating the yield condition as a discontinuous transition will cause immediate numerical problems. Instead, the transition must be modelled as a continuous transition, which may be done by adjusting Eq. 1 such that (Mitsoulis and Abdali, 1993)

$$\eta = \frac{\tau_y (1 - e^{-m\dot{\gamma}})}{\dot{\gamma}} + K\dot{\gamma}^{n-1}, \qquad [23]$$

where *m* is a 'smoothening parameter' to determine how rapid the transition from un-yielded to yielded flow occurs in terms of the value of the shear rate. With data from flow visualizations the value of this parameter can be determined by fitting the result with the numerical model.

The numerical modelling in this paper has been done using Comsol Multiphysics v5.2. Comsol Multiphysics enables user defined expressions of the apparent viscosity as a function of the shear rate, meaning any rheology model can be implemented in the flow model.

3. Results

3.1 Flow visualizations vs. analytical model in straight channel without restrictions

In this section results from flow visualizations, analytical models and numerical models are presented and compared. A straight channel with- and without restrictions have been considered. Figure 3 show measured velocity profiles across the channel; in order to compare the profiles the speed has been made dimensionless, scaled with the maximum value measured for respective grease. In Fig. 3a profiles for all three greases with NLGI grade 00 to 2 are shown, while in subfigure (b) only the velocity profile for the NLGI2 grease is shown (dotted curve) together with the analytically obtained profiles (solid, dashed, and dash-dotted respectively) for different cases explained below.

From Fig. 3a it follows that the two thicker greases have a distinct plug profile while the NLGI00 grease

have a parabolic velocity profile similar to the profile of a Newtonian fluid. The yield point (cf. Eq. 17) is around 0.3 mm from the side walls for the NLGI1 and 2 greases, while the NLGI00 grease is continuously sheared throughout the channel forming the characteristic parabola. An interesting observation is that when extrapolating the velocity profiles in subfigure (a) towards the walls, the velocity does not approach zero which it should do for the case of a no slip condition at the wall. This result indicates that there is a slip layer close to the walls where the velocity gradient is much larger compared to outside of this layer.

The effect increases with the NLGI number. The velocity profiles in this thin layer have not been measured in detail, but Westerberg et al. (2010) showed that when zooming into this region the velocity continuously approaches zero with increasing magnification of the microscope objective. This observation indicates that the grease is continuously sheared in this layer and that the velocity ultimately should reach zero at the wall (the wall is stationary). If the slip layer is comprised of base oil due to phase separation (bleeding), there is a thin layer close to the wall governed by a Newtonian rheology followed by a transition to the bulk grease at the end of the slip layer. The difference in slip effect between the three greases as seen in Fig. 3a indicate that the thickener concentration has a direct impact; the rate of shear is of the same order of magnitude for all greases, meaning the effect of shear on phase separation on respective grease is comparable. Fig. 3c shows that with an increasing shear in the flow the slip effect reduces together with a velocity profile approaching a parabola; i.e. with an increased shear rate the flow approaches a Newtonian behaviour. This is in line with the property of the grease viscosity which due to the increased disruption of the fibre network in the soap, approaches the base oil viscosity as introduce above.

Comparing the analytical model with the flow visualizations for the NLGI2 grease (Fig. 3b), three different cases have been considered. First, the slip velocity included in the model is a free parameter and its value be obtained by matching the model with the first data point of the measured velocity close to the wall. The same yields for the parameters in the H-B rheology model and the pressure drop. The latter can be approximated through the measured driving pressure and the length of the channel; caution must however be considered as one definitive error source is the actual pressure drop between the entry of the flow in the channel, and the exit. The driving pressure is measured before the elbow bend in the connection between the tube and the setup, and there is a pressure drop as the grease flow through the elbow entering the channel.

In Fig. 3b the solid line which shows a perfect match between the measured profile and the model, the measured (approximated) pressure gradient has been used while the values of the yield stress (τ_0) and grease consistency (*K)* have been adjusted to obtain the fit. Comparing the fitted values with the measured values in Tab. 1 we note a rather significant difference. One immediate possible explanation of this result is that the observed slip effects affect the measurements in the rheometer. The obtained values in the cone-plate rheometer are obtained in a similar way as in the fitting in this paper: the rheometer's software performs a best fit between the measured shear rate/shear stress relation and the actual rheology model's shear rate/shear stress relation. The shear is assumed to be continuous throughout the grease sample in the gap, meaning disruptions like slip effects or shear banding (Li et al., 2014) will affect the measurements. A relevant question then is how trustworthy the measurements in a rheometer are for the case of present non-ideal effects such as wall slip and shear banding.

The dash-dotted line in Fig. 3b represents the analytical model where the measured values of τ_0 and *K* have been used, and the value of the pressure drop included in the model has been fitted to match the maximum speed (plug) in the channel. As shown, the model does not fit the location of the yield point in the flow. In the dash-labelled graph the measured values of the pressure drop and parameters in the H-B rheology model have been used (velocity scale on the right y-axis). This yields a strong deviation compared to the measured velocity profile both in shape and absolute value. The results presented in this paragraph indicate that the actual pressure drop in the channel is less than the calculated pressure drop from the measured driving pressure.

3.2 CFD modelling of grease flow in straight channel with a step- and double lip restriction

The main objective of the CFD part of this study is to validate the model with the analytical results and measured velocity profiles, and thereby ensuring the quality and trust of the numerical simulations including the accuracy of the applied rheology model. With a working model flow cases with higher pressure drop in the channel with restrictions is analysed.

As introduced in §2.3 Comsol Multiphysics v5.2 has been used to model the grease flow. The grease is

described as a single-phase continuous Herschel-Bulkley fluid. The equations governing the flow is the equation of motion (Navier-Stokes equation) and the continuity equation respectively, which for a stationary flow reads (as implemented in Comsol Multiphysics)

$$\rho\mathbf{u}\cdot\nabla\mathbf{u} = -\nabla p + \nabla\cdot\mu\left(\nabla\mathbf{u} + (\nabla\cdot\mathbf{u})^T\right) \qquad \text{[23a-b]}$$
$$\nabla\cdot\mathbf{u} = 0\,.$$

Continuity yields that the last term in Eq. 23a vanishes, and the equation is the same as Eq. 3 used in the analytical model with the difference that the stress tensor is expressed in terms of the apparent viscosity. The relation between the viscosity, shear rate and the grease yield stress value is then governed by the Herschel-Bulkley rheology model (Eq. 1). Comsol Multiphysics has a built-in variable (*spf.sr*) representing the shear rate, enabling user defined rheology models – which in turn introduces a great flexibility in the modelling work. The boundary conditions at the inlet and the outlet are set to the fixed pressures with no viscous stresses, i.e. $p = p_{in}$ and $p = p_{out}$ at the in- and outlet respectively. Also, no viscous stresses in the normal direction is applied, yielding $\mathbf{n}\cdot[\mu(\nabla\mathbf{u}+(\nabla\mathbf{u})^T)] = 0$. In order to study the effect of the pressure drop on the flow a parametric solver has been used to vary p_{in} from 30 kPa to 250 kPa to match the study by Li et al. (2012). All other boundaries for simplicity impose the no slip condition $\mathbf{u} = 0$. Comsol Multiphysics however also enable a specified slip length and slip velocity in connection to the solid boundaries which can be applied to obtain a best possible fit between the model and experimental results where slip is shown present (Fig. 3). The slip velocity does however effectually only cut off the profile close to the wall and does not affect the shape of the velocity profile.

Figure 2 shows the different 2D channel configurations considered in this study. The channel length is 49 mm and in Fig. 4 the centre region is shown. There are three zones considered in the channel with a step restriction: zone 1, 2 and 3 indicating location before restriction, at the restriction and after restriction respectively. For the double restriction position 1 and position 2 are on the tip of first restriction and in the middle of the two restrictions respectively.

3.2.1 Velocity profiles and velocity surface plots

3.2.1.1 Channel without restrictions

Figure 6 shows the fully developed velocity profiles in the straight channel without restrictions for varying pressure drops and greases. Comparing the evolution of the velocity profiles for the increasing pressure and NLGI grade (the latter incresasing from subfigures a-c), it is clear that the shape becomes more parabolic . The NLGI00 grease (a) does however due to its negligible yield stress experience no plug region but keeps a parabolic form. These reults are also aligned with the measured profiles in Fig. 3 which in turn match the findings from the analytical model. With an increaseing pressure drop Eq. 17 lead to an increased value of y_l, meaning the location of the yield point appraches the center of the channel; i.e. a parabolic shape of the velocity profile. In terms of the stresses in the flow, these results mean that the yield behavior of the grease is reduced with increasing shear in the flow.

Recalling the visco-elastic properties of the grease, the thickener fibre structure is responsible for the elastic behavior at low shear rates including the yield behavior. As the shear rate increases the fiber network will be disrupted and aligned with the main shear direction, and consequently have less impact on the viscosity of the grease. And ultimately, as instroduced in §2.1, for infinite shar rates the grease viscosity approaches the base oil viscosity which is not dependent on the shar rate; i.e. the base oil has a Newtonian rheology.

Investigating the actual pressure drop in the channel, the profiles in Fig. 3a correspond to a driving pressure for the NLGI1 and NLGI2 grease of 100- and 150 kPa respectively. Comparing these velocity profiles with the corresponding profiles in it is noted that the plug region length is of the same order as in the measured profiles using µPIV, indicating that the measured driving pressure is representative to the actual pressure drop in the channel. To conclude the results from the channel without restrictions, there is a good agreement between the numerical- and analytical model, and the measured velocity.

3.2.1.2 Channel with step restriction

Continuing with the channel with a step restriction, Fig. 2b-c, three zones have been selected for the channel with one flat restriction: before the step, at the top of the step, and after the step respectively. Figure 7 shows the simulated velocity field for the NLGI2 grease at 250 kPa (maximum velocity 1.02 m/s). Subfigures a-c shows the velocity at respective position (zone 1-3 in Fig. 2b). The flow rate in the channel is constant which together with continuity in the flow yields an increased velocity as the step is approached, and to at the top of the step approach a pure straight channel flow. Subfigure a and c indicate symmetry in the flow before and after the step and in order to investigate this further the velocity profiles

upstream- and downstream of the are plotted; see Figs. 8-9. From Figs. 9a,e it follows that the flow is fully developed upstream of the step and that the flow has retained its upstream profile at corresponding distance downstream of the step. Fig. 9b shows the transition flow as the upstream corner of the step is rounded, while Fig. 9d shows the mirrored case when the flow is leaving the restriction. Fig. 9c shows the unrestricted flow at the top of the step. These results conclude that the flow is completely symmetric along a symmetry line drawn at the center of the step restriction. The effect of increased shear on the flow is also shown in the transition as the flow rounds the corner of the step, going from a fully developed plug profile, approaching a parabola, and eventually when stabilizing at the top of the step reaching a plug formation once again. The behavior of the thinner greases was found to be analogous in terms of symmetry and development of the velocity profiles considering the difference in the channel without restrictions. With a less pronounced yield stress the plug flow effect is decreasing with the NLGI grade.

(c)

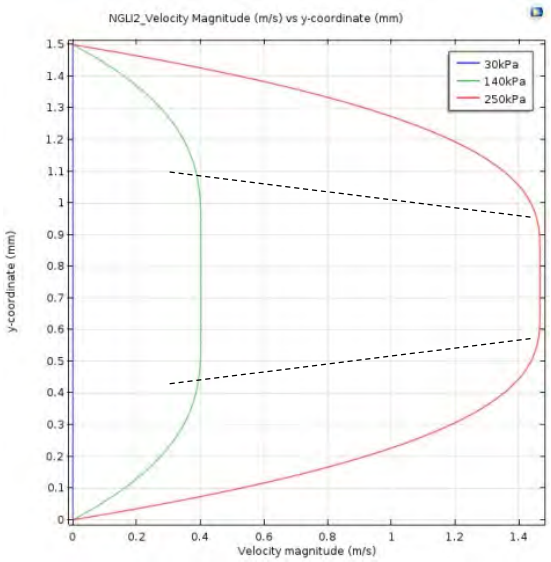

Figure 6: Velocity profiles (fully developed) of (a) NLGI00 (b) NLGI1 and (c) NLGI2 greases in the straight channel without restrictions. The pressures represent the pressure drop between inlet and outlet, and the dashed lines shows the evolution of the plug region with increasing pressure.

(a)

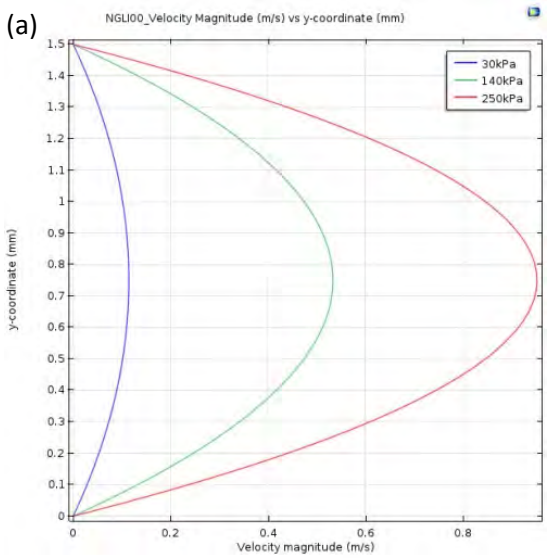

(b)

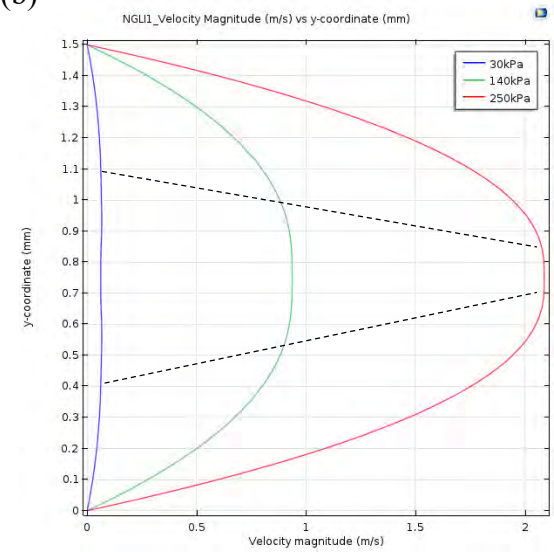

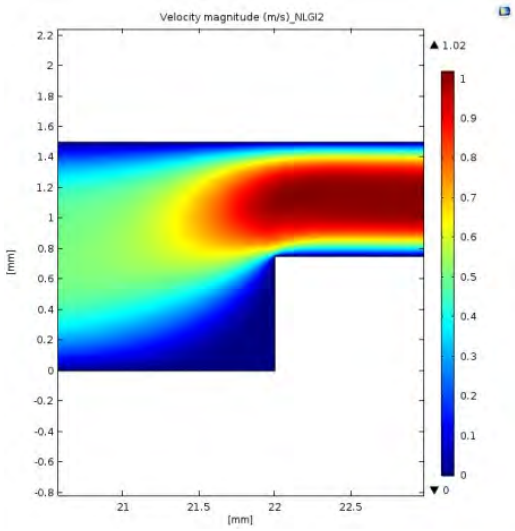

(a)

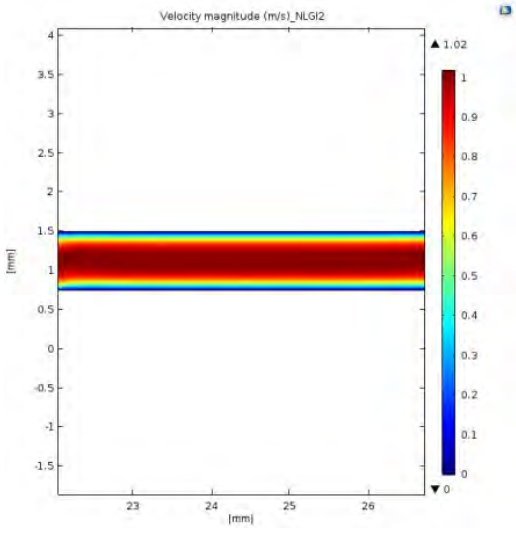

(b)

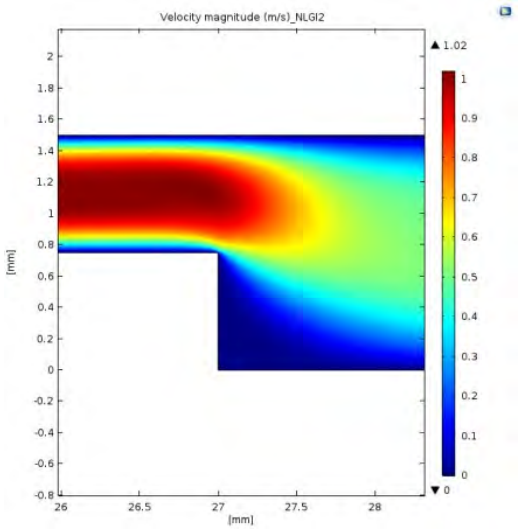

(c)

Figure 7: Average velocity field of NLGI2 grease at 250 kPa

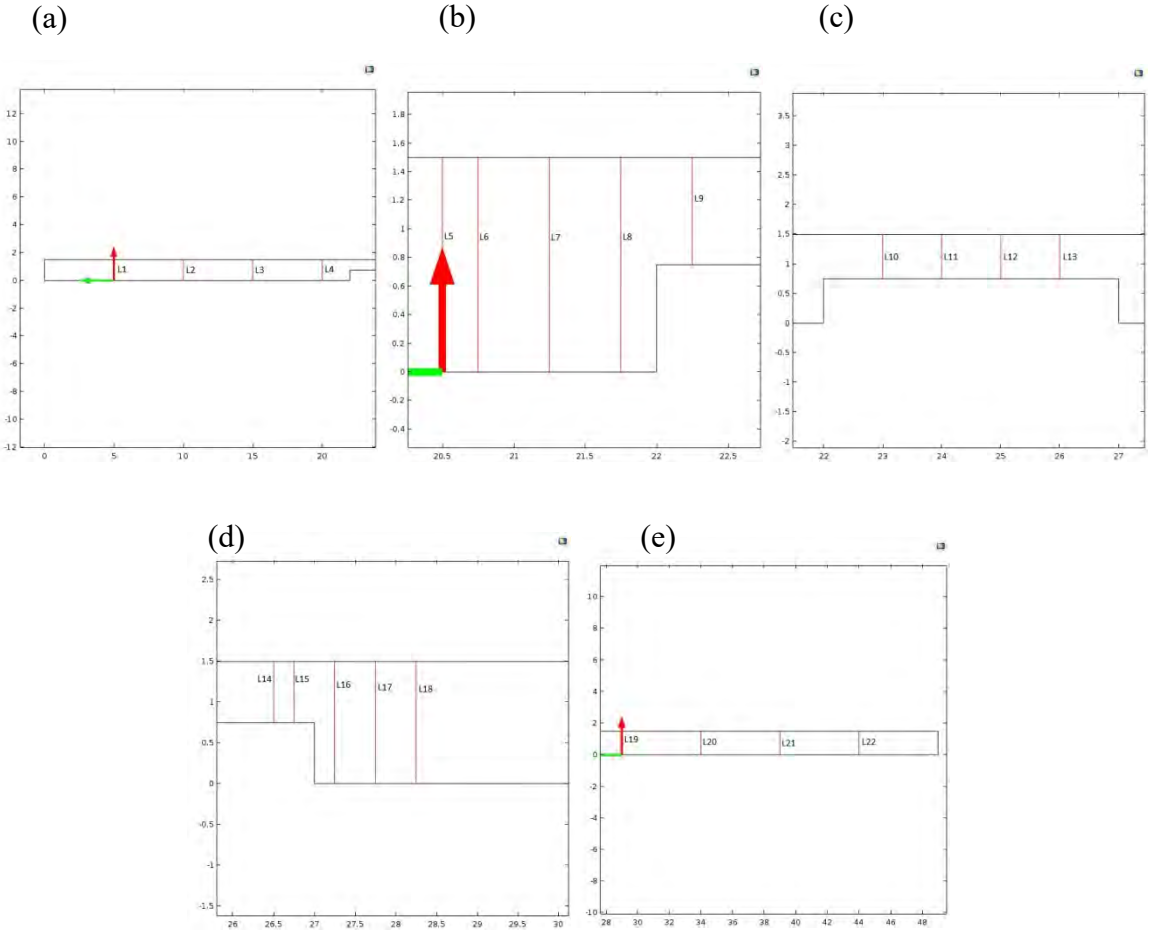

Figure 8: Sketches of cutline (a) L1, L2, L3, L4 along the inlet, (b) zone 1: L5, L6, L7, L8, L9 before the restriction, (c) zone 2: L10, L11, L12, L13 in the restriction, (d) zone 3: L14, L15, L16, L17, L18 after the restriction and (e) L19, L20, L21, L22 along the outlet

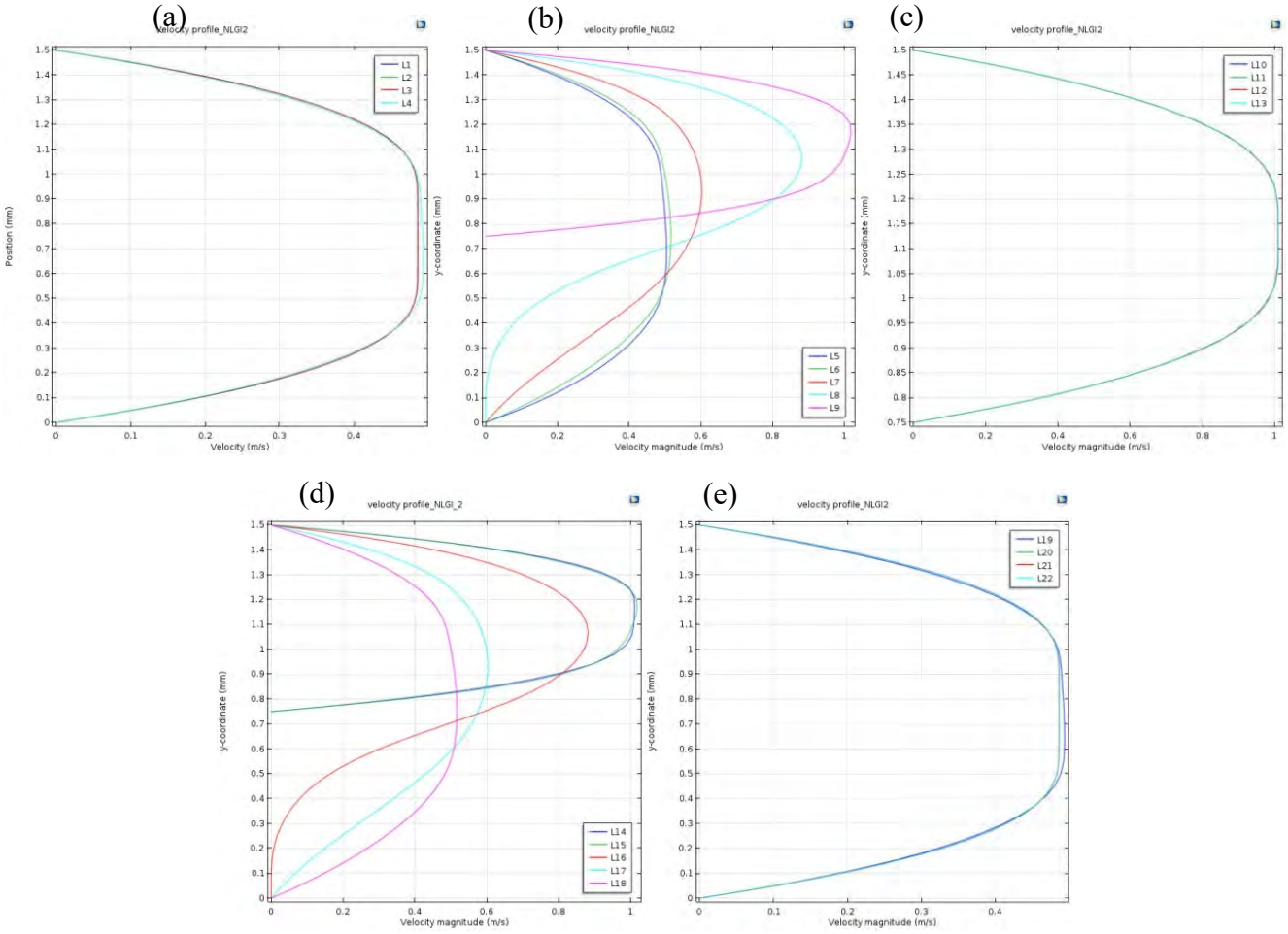

Figure 9: Velocity profiles of the NLGI2 grease at the position of the cut lines presented in Fig. 8. Each subfigure in this figure correspond to the same set of cut-lines as in corresponding subfigure in Fig. 8.

3.2.1.3 Channel with double lip restriction

For the channel with double the restriction, the distance between the two restriction tips is 1.5 mm, the minimum gap height 0.9 mm, and the maximum gap height between the restrictions is 1.5 mm as shown in Fig. 2c. The maximum velocity is observed above the two restrictions where the gap height is small as found in Li et al. (2012).

Figure 10a-b show the velocity magnitude at 30 kPa and 250 kPa for the NLGI2 grease. In line with previous results a higher-pressure drop results in a higher velocity in the flow. Of specific interest here is to investigate the *flow depth* (Li et al., 2012) between the restrictions, as particles stuck between the restrictions – depending on the flow depth - either will remain stuck or be dragged along with the flow. In terms of application where this type of flow is present, the flow depth is important for how contamination particles (like road dust) and wear particles are transported. To capture the behaviour of grease flow depth at high pressure, Fig 10b has been redrawn considering the same scale as for the lower pressure (Fig. 10a). It follows that most of the domain consists of fully yielded grease.

Figure 11 shows the velocity profiles for the three greases at position 1 and position 2 as defined in Fig. 2c. It can be observed that the NLGI00 grease has a more parabolic flow compared to the NLGI1 and NLGI2 grease through the position 1 as is suspected based on previous results.

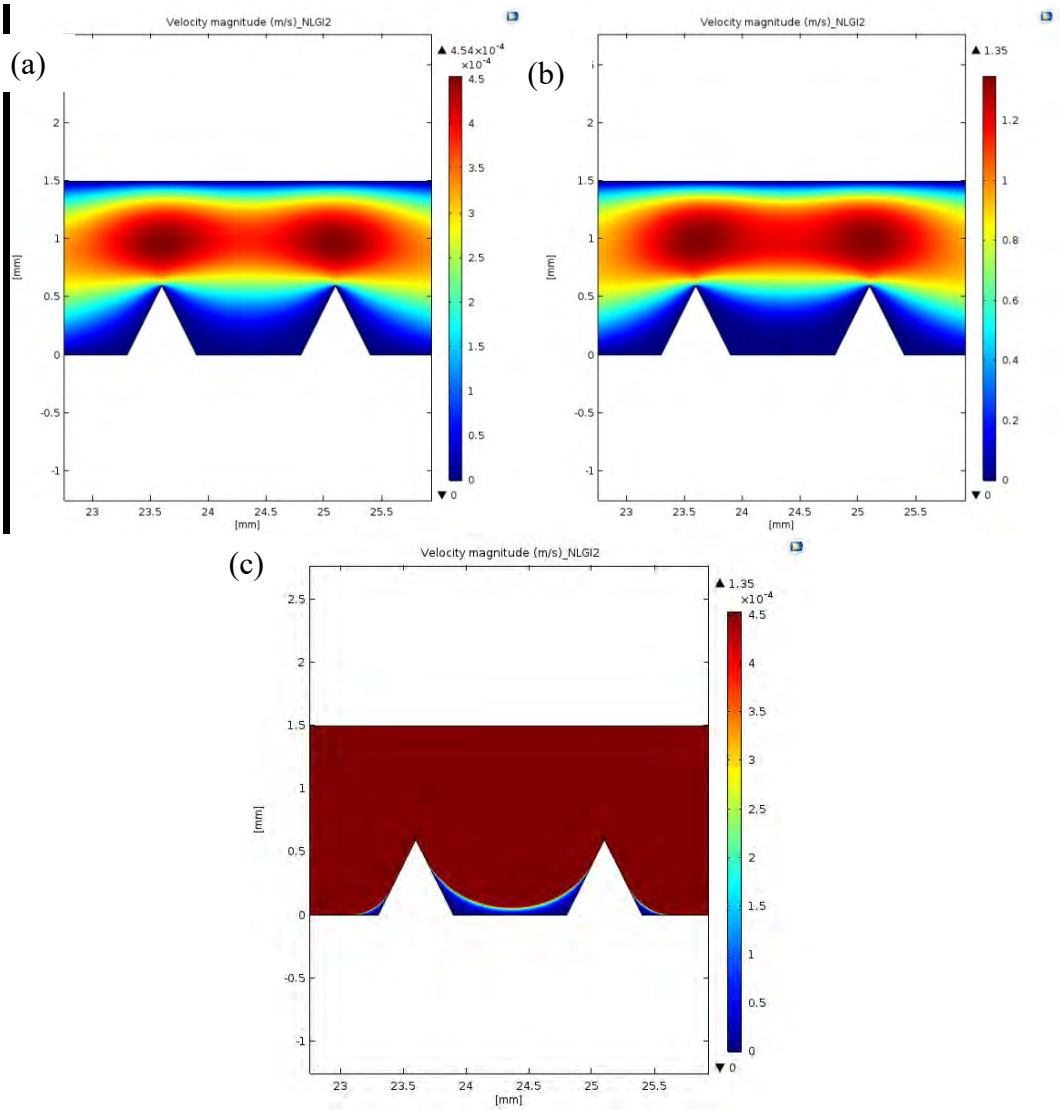

Figure 10: The average velocity field for the NLGI2 grease at (pressure drop): (a) 30 kPa, (b) 250 kPa, (c) 250 kPa with same range of colour bar as in (a).

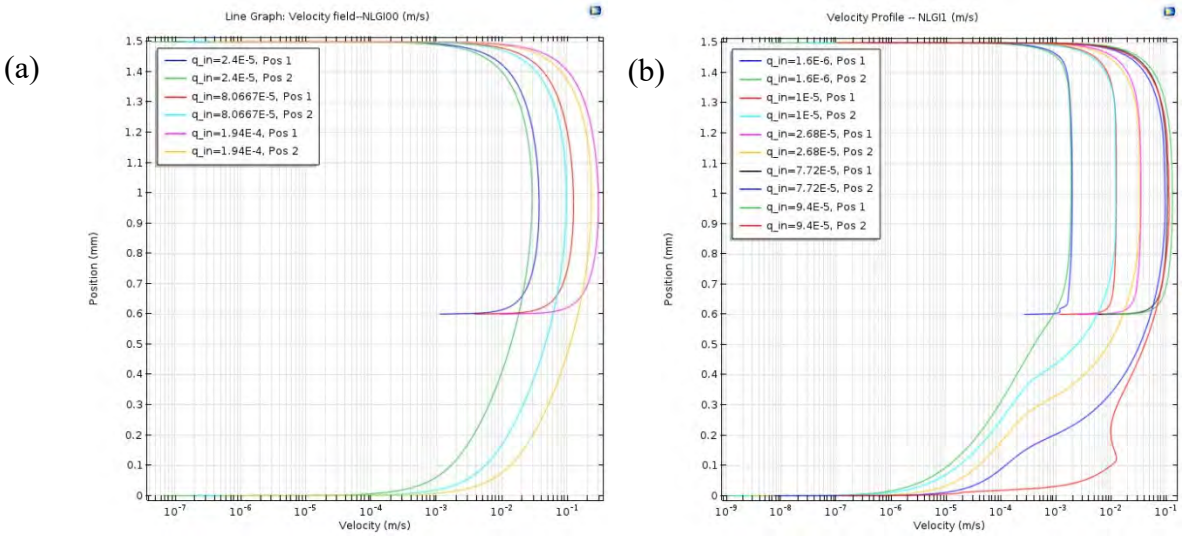

(c)

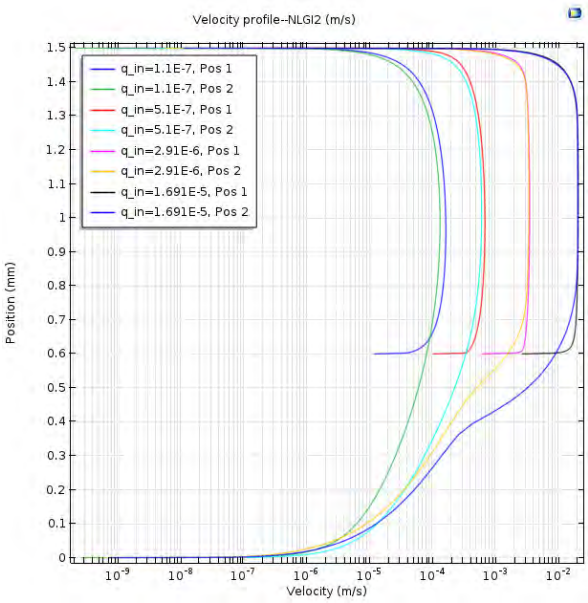

Figure 11: Velocity profile measured at position 1 and position 2 in Fig. 2c: (a) NLGI00 grease, (b) NLGI1 grease, (c) NLGI2 grease. The flow rate *q* is the flow across the channel height for each corresponding position.

4. Concluding remarks

This paper presents a combined approach where analytical modelling, flow visualizations using micro Particle Image Velocimetry, and numerical modelling using Computational Fluid Dynamics has been used to analyse the flow motion of lubricating greases in channels with- and without restrictions. The CFD model has been validated with the analytical model and measured velocity profiles, enabling flow simulations in more complicated geometries where analytical models cannot be obtained, nor flow visualizations.

It was found that the simulations match the experiments and analysis well, capturing the yield- and shear rate-dependent characteristics of lubricating grease flow. The grease has been modelled as a single-phase Herschel-Bulkley fluid which was found to match well with the bulk motion of grease as measured in experiments.

5. References

- A.D. Bramhall and J.F. Hutton, Wall effect in the flow of lubricating greases in plunger viscometers, *British J. Appl. Phys.,* 11(8):363-371, 1960.
- P. Baart, B. Van der Vorst, P.M. Lugt, and R.A.J. Ostayen. Oil bleeding model for lubricating
- grease based on viscous flow through a porous microstructure. *Tribology Transactions,* 53(3):340-348, 2010.
- C. Balan and J.M. Franco. Influence of geometry on the transient and steady flow of lubricating greases. *STLE Tribology Transactions*, 44(1):53–58, 2001.
- H.A. Barnes and K. Walters. The yield stress myth. *Rheologica acta*, 24:323–326, 1985.
- H.A. Barnes. The yield stress - a review or 'panta roi' - everything flows? *J. Non-Newtonian Fluid Mech.*, 81:133–178, 1999.
- R. Czarny, The influence of surface material and topography on the wall effect of grease, *Lub. Sci.*, 14(2):255-274, 2002.
- R. Czarny and H. Moes. Some aspects of lubricating grease flow. *Proc. of the 3rd Int. Cong. Trib. Eurotrib 8*, 3:68–85, 1981.
- R. Czarny. The influence of surface material and topography on the wall effect of grease. *Lubrication Science*, 14-2:255–274, 2004.
- M. Gafitanu, D. Silicon, Ianus G., and D. Olaru. A general model for grease deterioration in ball bearings. *Proc. 6th Int. Congress on Tribology, EUROTRIB, Budapest*, 2:355–359, 1993.

- G.B. Froishteter, E.L. Smorodinskii, Y.L. Ishchuck, L.O. Yurtin, and N.V. Radionova. Calculation of hydraulic resistance in transport of lubricating greases through pipelines. *All Union Scientific Research and Design Institute of the Petroleum Refining and Petrochemical Industry, Translated from Khimiya i Technologiya Topliv i Masel, No, 2 pp.34-37, 1976*, (UDC 665.521.5:532.542):129–133, 1976.
- L. Gershuni, M.G. Larson, and P.M. Lugt. Replenishment in rolling bearings. *STLE Tribology Transactions*, 51:643–651, 2008.
- G.M. Gow. The CEY to grease rheology. *Transactions of Mechanical Engineering, The Institution of Engineers, Australia, Special Issue Tribology*, ME16(3):202–205, 1991.
- G. Gow. Lubricating grease. In R. M Mortier and S. T. Orszulik, editors, *Chemistry and Technology of Lubricants*. 1994. ISBN 0-7514-0117-X.
- T.E. Karis, R.-N. Kono, and M. Jhon. Harmonic analysis in grease rheology. *Journal of Applied Polymer Science*, 90:334–343, 2003.
- E. Kleinlein. *Proc.3rd. Int. Trib. Congress, Eurotrib'81*, II:208, 1981.
- P.-O. Larsson, B. Jacobson, and E. Höglund. Oil drops leaving an EHD contact. *Wear*, 179:23–28, 1994.
- J. Li, E. Höglund, L.G. Westerberg, T. Green, T. Lundström, P.M. Lugt and P. Baart. µPIV measurements of grease velocity profiles in channels with two different types of flow restrictions. *Trib. Int.* 54:94-99, 2012.
- J. Li, L.G. Westerberg, E. Höglund, P. Lugt, and P. Baart. Lubricating grease flow and boundary layers in a concentric cylinder configuration. *Trib. Trans.* 57(6):1106-1115, (2014).
- P.M. Lugt. A review on grease lubrication in rolling bearings. *STLE Tribology Transactions*, 52(4):470-480, 2009.
- P.M. Lugt, S. Velickov, and J.H. Tripp. On the chaotic behaviour of grease lubrication in rolling bearings. *Tribology Transactions*, 52:581-590, 2009.
- P.M. Lugt, Grease lubrication in rolling bearings, *Wiley & Sons*, 2013.
- P.M. Lugt, Modern advancements in lubricating grease technology, *Trib. Int.* 97:467-477, 2016.
- H.E. Mahncke and W. Tabor. A simple demonstration of flow type in greases.
- *Lubrication Engineering*, Jan-Feb.:22–28, 1955.
- B. Manshoor, M. Jaat, Z. Izzuddin, and K. Amir, CFD analysis of thin film lubricated journal bearing, *Proc. Eng.*, 68:56-62, 2013.
- R. Mas and A. Magnin. Steady shear and dynamic viscosity relation for yield stress fluids. *Rheologica Acta*, 36:49–55, 1997.
- E. Mitsoulis, and S.S. Abdali, Flow Simulation of Herschel-Bulkley Fluids through Extrusion Dies, *The Canadian Journal of Chemical Engineering*, 71:147-160, 1993.
- A.V. Radulescu, D. Bonneau, and M. Hajjam. A theoretical study of two-dimensional grease flow in regions with discontinuities. *Lubrication Science*, 15(2):163–171, 2003.
- M.T. van Zoelen, C. H. Venner, and P. M. Lugt. Free surface thin layer flow on bearing raceways. *ASME Journal of Tribology*, 130(2):021802–1–021802–10, 2008.
- M.T. van Zoelen, C.H. Venner, and P.M. Lugt. Centrifugal effects and free surface thin layer flow in roller bearings. *STLE Tribology Transactions*, 53(3):297-307, 2010.
- M.T. van Zoelen. *Thin Layer Flow in Rolling Element Bearings*. PhD thesis, University of Twente, The Netherlands, ISBN 978-90-365-2934-1, December 2010.
- G.V. Vinogradov, G.B. Froishteter and K.K. Trilisky, The generalized theory of flow of plastic disperse systems with account of the wall effect, *Rheol. Acta*, 17(2):156-165, 1978.
- L.G. Westerberg, T.S. Lundstrom, E. Höglund, and P.M. Lugt. Investigation of grease flow in a rectangular channel including wall slip effects using micro Particle Image Velocimetry. *STLE Tribology Transactions*, 53(4):600-609, 2010.
- V. Wikstrom and E. Höglund. Starting and steady-state friction torque of grease lubricated rolling element bearings at low temperatures - part II: Correlation with less-complex test methods. *STLE Tribology Transactions*, 39(3):684–690, 1996.
- A.E. Yoesif. Rheological properties of lubricating greases. *Wear*, 82:13–25, 1982.
- H. Åstrom and E. Höglund. Rheological properties of lithium, lithium complex and sodium greases. *Journal of Synthetic Lubrication*, 10(3):225–236, 1993.